

Imaging Nanostructures by Single-Molecule Localization Microscopy in Organic Solvents

Antonio Aloï,[†] Andreas Vargas Jentzsch,[†] Neus Vilanova,[†] Lorenzo Albertazzi,[‡] E. W. Meijer,[†] and Ilja K. Voets^{*†}

[†]Department of Chemical Engineering and Chemistry, Institute for Complex Molecular Systems, Eindhoven University of Technology, P.O. Box 513, Eindhoven 5600 MD, The Netherlands

[‡]Nanoscopia for Nanomedicine Group, Institute for Bioengineering of Catalonia (IBEC), C. Baldori Reixac 15-21, Barcelona 08028, Spain

S Supporting Information

ABSTRACT: The introduction of super-resolution fluorescence microscopy (SRM) opened an unprecedented vista into nanoscopic length scales, unveiling a new degree of complexity in biological systems in aqueous environments. Regrettably, supramolecular chemistry and material science benefited far less from these recent developments. Here we expand the scope of SRM to photoactivated localization microscopy (PALM) imaging of synthetic nanostructures that are highly dynamic in organic solvents. Furthermore, we characterize the photophysical properties of commonly used photoactivatable dyes in a wide range of solvents, which is made possible by the addition of a tiny amount of an alcohol. As proof-of-principle, we use PALM to image silica beads with radii close to Abbe's diffraction limit. Individual nanoparticles are readily identified and reliably sized in multicolor mixtures of large and small beads. We further use SRM to visualize nm-thin yet μm -long dynamic, supramolecular polymers, which are among the most challenging molecular systems to image.

The introduction and use of super-resolution optical fluorescent microscopy (SRM) has opened the door to a better understanding of living cells and organisms. Techniques such as SSIM, STED, RESOLFT, (d)STORM, (f)PALM (see SI for a detailed description) give access to length scales otherwise inaccessible to optical microscopy shedding new light on structure–function relationships of living matter with unprecedented detail.¹ SRM circumnavigates the diffraction barrier while profiting from many of the advantages inherent to optical microscopy, like multicolor and target-specific labeling. This is what makes SRM a powerful tool to study biological systems and complementary to well-established characterization methods such as X-ray crystallography, nuclear magnetic resonance (NMR), and electron microscopy (EM).² Numerous practical applications of SRM have been demonstrated in recent years. Illustrative examples include the mapping of neurons³ protein-driven chromosome organization,⁴ and the periodic structure of actin and spectrin in axons.⁵

Small molecules that self-assemble to form long unidimensional structures reminiscent of natural systems also represent a fascinating class of supramolecular organization.⁶ Since widespread interest in biomaterials has catalyzed the design of

molecular motifs for assembly into such supramolecular polymers in aqueous media,⁷ some of us revealed the structure and exchange dynamics of supramolecular polymers in water using single-molecule localization microscopy (SMLM).⁸ However, the majority of these synthetic systems are only soluble in organic, nonprotic media, like alkanes or chlorinated solvents. Preliminary steps toward super-resolution imaging in organic solvents have been taken to map living crystallization-driven block copolymer self-assembly in cyclohexane⁹ and colloidal nanostructures in material science.¹⁰ Inspired hereby, we decided to investigate the exciting possibility of expanding the scope of SMLM to organic solvents. Here we report on the photophysical properties of commercially available PALM dyes in organic solvents and their utility for SRM imaging of nanoparticles and synthetic supramolecular systems in organic media.

Essential for PALM (as for any SMLM technique) is the choice of the most suitable fluorophore. Among the various PALM dyes reported in the literature, there are only a few which chemistry is not necessarily affected by the solvent.¹¹ These, however, have important limitations, such as the colorful and potentially toxic nature of the byproducts (e.g., nitrobenzyl derivatives). At present, PALM dyes based on diazoketo chemistry and commercially available (e.g., Cage-552, Cage-635) are well-known and commonly used on commercial and custom microscopes.

Unfortunately, photolysis of Cage-552 (Abberior) in typical organic solvents such as CHCl_3 , toluene, and acetonitrile resulted almost exclusively in nonfluorescent products (Figure S2), and as a result, PALM experiments in organic solvents failed. While the photoreaction and the subsequent Wolff rearrangement of the caged dyes likely proceed in most solvents, the last step in the reaction mechanism that leads to the fluorescent form requires a nucleophilic attack on the formed ketene, limiting its use to nucleophilic solvents like MeOH or water.¹² To circumvent this limitation, we simply added small amounts of alcohol to the organic solvents. Gratifyingly, addition of tiny percentages ($\leq 2\%$) already recovers significant fluorescence in every solvent tested (48–325% relative to water; see Figure S2 for the effect of different

Received: December 31, 2015

Published: February 17, 2016

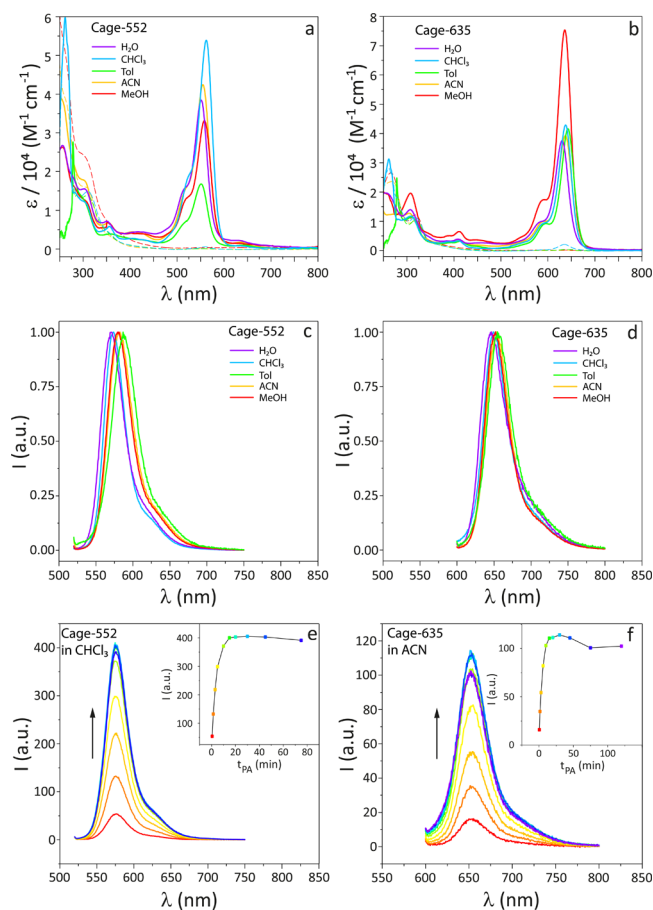


Figure 1. (a,b) Absorption spectra of the caged rhodamine Cage-552 and Cage-635, respectively, before (dashed lines) and after (solid lines) UV photoactivation ($\lambda_{\text{PA}} = 354 \text{ nm}$), collected in different organic solvents (as indicated) in the presence of 2% v/v of MeOH, and in Milli-Q water. (c,d) Emission spectra of Cage-552 and Cage-635, respectively, collected after UV photoactivation in the same solvents (6–60 min; see SI, section 4.1.2 for details). (e,f) Photoactivation kinetics of Cage-552 in CHCl_3 and Cage-635 in ACN, respectively, showing the evolution of the fluorescence emission as a function of UV light exposure time t_{PA} .

amounts of added MeOH). We decided to add 2% v/v MeOH for SMLM imaging in organic media, which ensures a high yield

Table 1. Photophysical Properties of Cage-552 and Cage-635 in a Series of Organic Solvents^a and in Water

solvent	closed form (CF)		fluorescent product (FP) ^b			
	abs. max (nm)	$\epsilon / 10^3 (\text{M}^{-1} \text{cm}^{-1})$	abs. max (nm)	$\epsilon / 10^3 (\text{M}^{-1} \text{cm}^{-1})$	em. max (nm)	ϕ^c
Cage-552	Tol	309	14	551	17	0.16
	MeOH	301	24	558	33	0.40 ^d
	ACN	307	16	555	42	0.11
	CHCl_3	310	15	562	54	0.75
	H_2O	324	19	551	38	0.23
Cage-635	Tol	317	10	643	42	0.27
	MeOH	318	12	636	75	0.54 ^d
	ACN	316	10	637	39	0.42
	CHCl_3	317	11	638	43	0.79
	H_2O	323	16	630	38	0.27

^aThe selected solvents cover the main families (i.e., chlorinated, alcohols, aromatics, aliphatic) of organic solvents and span over a broad range of dielectric constants. 2% v/v of MeOH was added to toluene, acetonitrile, and chloroform. ^bPhotophysical properties of the reaction mixture after UV photoactivation (6–60 min; see SI, section 4.1.2). ^cRelative quantum yield using the same dye in MeOH corresponding to the reaction mixture after photolysis. ^dLiterature value.¹³

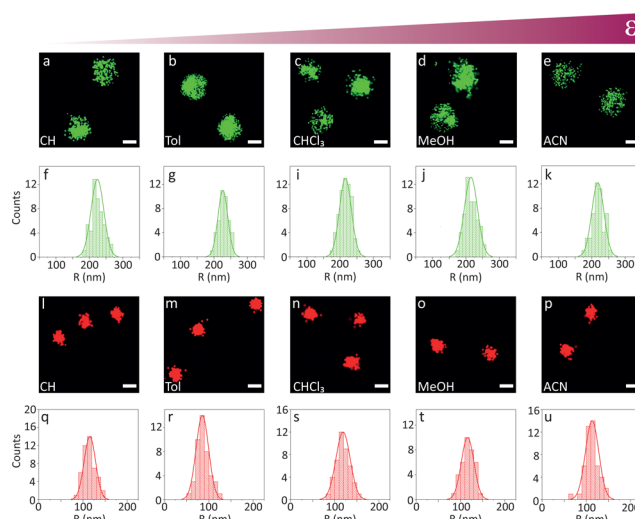


Figure 2. (a–e) and (l–p) Super-resolved images of silica colloids ($R \sim 220 \text{ nm}$) labeled with Cage-552 and silica colloids ($R \sim 110 \text{ nm}$) labeled with Cage-635, respectively. The images were collected in different organic solvents (as indicated), covering a wide range of dielectric constant (ϵ). Scale bar 200 nm. (f–k) and (q–u) Corresponding distributions of the radii of the nanoparticles obtained by PALM image analysis (see Figure S13 for more details).

of the uncaging reaction without significantly affecting the properties of the solvent.

Next, we characterized the photophysical properties (i.e., absorption, emission, and relative quantum yield of fluorescence) of the caged dyes in aqueous and organic media covering the main families (i.e., chlorinated, alcohols, aromatics, aliphatic) of common organic solvents while spanning a wide range of dielectric constants, ϵ , varying between 2.38 (toluene) and 80.1 (water). In agreement with the published literature, both caged compounds show a large band in the region between 250–330 nm ($\epsilon = 14\text{--}24 \times 10^3 \text{ M}^{-1} \text{cm}^{-1}$) and a long and low intensity tail extending to 450 nm ($\epsilon \sim 7 \times 10^2 \text{ M}^{-1} \text{cm}^{-1}$) present in all solvents (Figure 1a,b). Upon irradiation with UV-A light ($\lambda_{\text{max}} = 354 \text{ nm}$, $7.0 \pm 0.5 \text{ mW cm}^{-2}$), a strong absorption band appears (Cage-552: $\sim 555 \text{ nm}$; Cage-635: $\sim 635 \text{ nm}$), confirming the formation of the uncaged and fluorescent adduct (Figures S8–S12). The corresponding

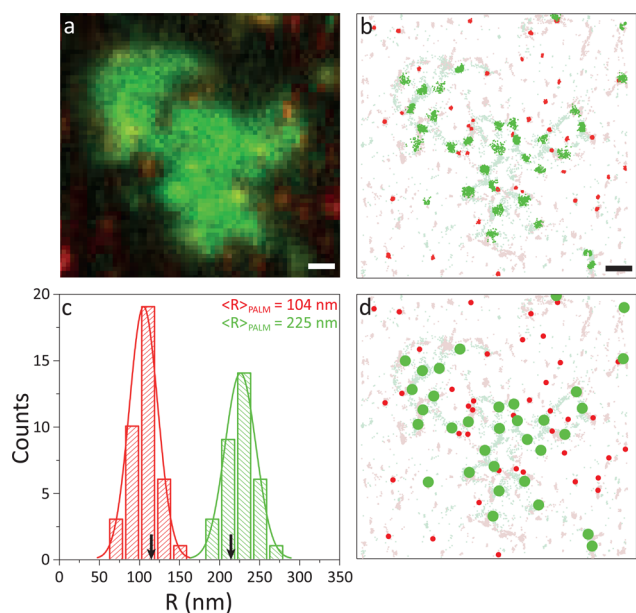


Figure 3. (a) Two-color wide-field image acquired in cyclohexane with 2% v/v isopropanol of a mixed cluster of colloidal particles of $R \sim 110$ nm labeled with Cage-635 and $R \sim 220$ nm labeled with Cage-552. (b) Super-resolved image of the field of view shown in (a). Scale bar $1 \mu\text{m}$. (c) Radii distribution of the nanoparticles identified and reconstructed in the mixed sample; black arrows indicate the mean radii determined by SEM. (d) Schematic representation of the beads identified in (b).

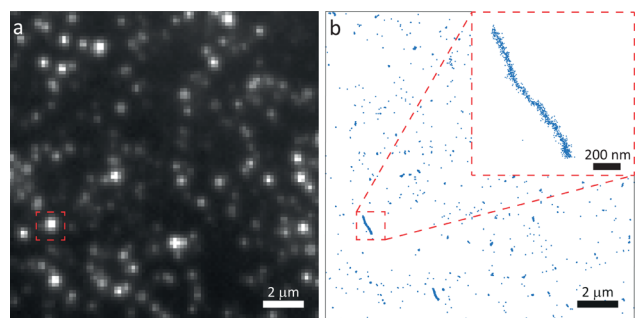


Figure 4. (a) Wide-field image of BTA fibers containing 5% Cage-552-labeled BTA acquired in cyclohexane with 2% v/v isopropanol. (b) Super-resolved image of the same field of view depicted in (a). The inset is a zoom-in on one of the fibers.

fluorescent emission (Figure 1c,d; Cage-552: ~ 580 nm; Cage-635: ~ 650 nm) shows small yet consistent shifts that are attributed to excited-state stabilization.¹⁴

To estimate the performance of the dyes in SMLM, we first explored the kinetics of uncaging. We find that 20 min UV-A irradiation of a 10^{-7} M solution suffices in most solvents to react all the uncaged molecules to either the dark¹³ or fluorescent product (Figure 1e,f; see Figures S3–S7 for the exact times and the remaining solvents). Second, the relative quantum yields of fluorescence (ϕ)¹⁵ were calculated using the reported values in MeOH as reference.¹³ Remarkably, the relative quantum yield in some organic solvents is significantly higher (up to 3-fold increase; see Tables 1 and S1) which should improve the localization accuracy.¹⁶

Having established the photophysical features of the dyes, we set out to image nanoparticles with radii R close to Abbe's diffraction limit by PALM in organic solvents. To this end, we synthesized monodisperse, spherical hydrophilic silica nano-

particles that were subsequently cofunctionalized with stearyl alcohol and either Cage-552 ($R \sim 220$ nm) or Cage-635 ($R \sim 110$ nm). PALM images were collected in the above-mentioned organic solvents with 2% v/v MeOH as well as cyclohexane (CH, in which the caged dyes are not soluble precluding photophysical characterization) to which 2% v/v isopropanol was added. Exemplary images in Figure 2 (panels a–e, l–p) show that both shape and size of the silica beads are clearly resolved in each solvent. Moreover, from the narrow distributions of their radii (Figures S14–S15), as depicted in Figure 2 (panels f–k and q–u), we obtain mean radii by PALM imaging that are in good agreement with mean radii calculated from scanning electron microscopy (SEM) images (Figure S1) ($<6\%$ difference).

Aiming to visualize a more complex multicomponent nanostructured material, we prepared composite aggregates of both colloids by evaporative self-assembly (Figures 3 and S16). The wide-field image in Figure 3a confirms colocalization of the Cage-552 and Cage-635 tagged beads within the clusters, but is unable to resolve the individual nanoparticles. By contrast, PALM microscopy (Figure 3b) reveals the disordered internal structure of the aggregate, resolves individual colloids, as represented by the cartoon in Figure 3d to guide the eye, and recovers the narrow size distributions of both particles centered on $\langle R \rangle_{\text{red}}: 104 \pm 18$ nm and $\langle R \rangle_{\text{green}}: 225 \pm 19$ nm (Figure 3c). The single-molecule localizations in Figure 3b that do not belong to a reconstructed particle are attributed to beads that are out-of-focus, as the evaporative self-assembly is not strictly 2D.

Encouraged by these promising results, we turned to an elusive system for standard imaging techniques due to their dynamic nature, size, and low imaging contrast: nm-thin yet μm -long, dynamic supramolecular polymers, so far studied mainly by spectroscopy and scanning-probe techniques.¹⁷ For this purpose we selected benzene 1,3,5-tricarboxamides (BTA). These small molecules are known to self-assemble by 3-fold hydrogen bonding into nanometer-sized, one-dimensional (1D) supramolecular polymers and have found a panoply of applications in material science.¹⁸ Figure 4 shows the super-resolved image of a BTA aggregate containing a small amount ($<5\%$) of monofunctionalized BTA with Cage-552 (Schemes S1–S2). Since the aggregates are $0.7\text{--}1.0 \mu\text{m}$ long and several nm's wide, their 1D morphology is clearly visible only in SMLM (Figure 4b). The supramolecular dimensions observed are in perfect agreement with data obtained previously on similar BTA supramolecular polymers by depolarized light scattering¹⁹ and atomic force microscopy.²⁰

In summary, we have demonstrated the possibility to perform super-resolution microscopy in a wide range of organic solvents with high accuracy. Narrow-size distributions and accurate mean radii were obtained by PALM for (mixed) nanoparticle dispersions even if the nanoparticles with radii close to Abbe's diffraction limit are in close contact. While the addition of an auxiliary nucleophile was essential in the experiments reported here, we foresee integration of the nucleophile into the dye structure in future work. Furthermore, we successfully visualized the morphology of dynamic, 1D supramolecular polymers composed of hydrogen-bonded small molecules, which are elusive to other imaging techniques. We expect that in situ visualization by SMLM of the structure and exchange dynamics of such supramolecular polymers in organic media will shed new light on their structure–function relations

and complex polymerization pathways. This will be reported in due time.

■ ASSOCIATED CONTENT

■ Supporting Information

Additional plots, data treatment description, and synthetic procedures. The Supporting Information is available free of charge on the ACS Publications website at DOI: 10.1021/jacs.5b13585.

■ AUTHOR INFORMATION

Corresponding Author

*I.K.Voets@tue.nl

Notes

The authors declare no competing financial interest.

■ ACKNOWLEDGMENTS

We would like to thank P. M. Gerris for preliminary experiments and Dr. N. J. van Zee for the synthesis of one of the BTA derivatives. The authors acknowledge The Netherlands Organization for Scientific Research (NWO-ECHO-STIP Grant 717.013.005, NWO-VIDI Grant 723.014.006), the European Union (FP7-PEOPLE-2012-ITN SOMATAI contract 316866), and the Dutch Ministry of Education, Culture and Science (Gravity program 024.001.035) for financial support.

■ REFERENCES

- (1) (a) Betzig, E.; Patterson, G. H.; Sougrat, R.; Lindwasser, O. W. *Science* **2006**, *313*, 1642–1645. (b) Hofmann, M.; Eggeling, C.; Jakobs, S.; Hell, S. W. *Proc. Natl. Acad. Sci. U. S. A.* **2005**, *102*, 17565–17569. (c) Huang, B.; Babcock, H.; Zhuang, X. *Cell* **2010**, *143*, 1047–1058. (d) Grotjohann, T.; Testa, I.; Leutenegger, M.; Bock, H.; Urban, N. T.; Lavoie-Cardinal, F.; Willig, K. I.; Eggeling, C.; Jakobs, S.; Hell, S. W. *Nature* **2012**, *478*, 204–208. (e) Eggeling, C.; Willig, K. I.; Sahl, S. J.; Hell, S. W. *Q. Rev. Biophys.* **2015**, *48*, 178–243. (f) Heilemann, M.; van de Linde, S.; Schüttelz, M.; Kasper, R.; Seefeldt, B.; Mukherjee, A.; Tinnefeld, P.; Sauer, M. *Angew. Chem., Int. Ed.* **2008**, *47*, 6172–6176.
- (2) (a) Shi, Y. *Cell* **2014**, *159*, 995–1014. (b) Wüthrich, K. *J. Biol. Chem.* **1990**, *265*, 22059–22062. (c) Bai, X.-C.; McMullan, G.; Scheres, S. H. W. *Trends Biochem. Sci.* **2015**, *40*, 49–57.
- (3) Lakadamyali, M.; Babcock, H.; Bates, M.; Zhuang, X.; Lichtman, J. *PLoS One* **2012**, *7*, e30826.
- (4) Wang, W.; Li, G. W.; Chen, C.; Xie, X. S.; Zhuang, X. *Science* **2011**, *333*, 1445–1449.
- (5) Dempsey, G. T.; Vaughan, J. C.; Chen, K. H.; Bates, M.; Zhuang, X. *Nat. Methods* **2011**, *8*, 1027–1036.
- (6) Aida, T.; Meijer, E. W.; Stupp, S. I. *Science* **2012**, *335*, 813–817.
- (7) Matson, J. B.; Stupp, S. I. *Chem. Commun.* **2012**, *48*, 26–33.
- (8) Albertazzi, L.; van der Zwaag, D.; Leenders, C. M. A.; Fitzner, R.; van der Hofstad, R. W.; Meijer, E. W. *Science* **2014**, *344*, 491–495.
- (9) Boott, C. E.; Laine, R. F.; Mahou, P.; Finnegan, J. R.; Leitao, E. M.; Webb, S. E. D.; Kaminski, C. F.; Manners, I. *Chem. - Eur. J.* **2015**, *21*, 18539–18542.
- (10) (a) Harke, B.; Ullal, C. K.; Keller, J.; Hell, S. W. *Nano Lett.* **2008**, *8*, 1309–1313. (b) Friedemann, K.; Turshatov, A.; Landfester, K.; Crespy, D. *Langmuir* **2011**, *27*, 7132–7139.
- (11) (a) Grimm, J. B.; Sung, A. J.; Legant, W. R.; Hulamm, P.; Matlosz, S. M.; Betzig, E.; Lavis, L. D. *ACS Chem. Biol.* **2013**, *8*, 1303–1310. (b) Lord, S. J.; Conley, N. R.; Lee, H.-L. D.; Samuel, R.; Liu, N.; Twieg, R. J.; Moerner, W. E. *J. Am. Chem. Soc.* **2008**, *130*, 9204–9205.
- (12) Belov, V. N.; Wurm, C. A.; Boyarskiy, V. P.; Jakobs, S.; Hell, S. W. *Angew. Chem., Int. Ed.* **2010**, *49*, 3520–3523.

(13) Belov, V. N.; Mitronova, G. Y.; Bossi, M. L.; Boyarskiy, V. P.; Heibisch, E.; Geisler, C.; Kolmakov, K.; Wurm, C. A.; Willig, K. I.; Hell, S. W. *Chem. - Eur. J.* **2014**, *20*, 13162–13173.

(14) Suppan, P. J. *Photochem. Photobiol., A* **1990**, *50*, 293–330.

(15) Resch-Genger, U.; Rurack, K. *Pure Appl. Chem.* **2013**, *85*, 2005–2026.

(16) Gelles, J.; Schnapp, B. J.; Sheetz, M. P. *Nature* **1988**, *331*, 450–453.

(17) (a) Ogi, S.; Sugiyasu, K.; Manna, S.; Samitsu, S.; Takeuchi, M. *Nat. Chem.* **2014**, *6*, 188–195. (b) Korevaar, P. A.; George, S. J.; Markvoort, A. J.; Smulders, M. M. J.; Hilbers, P. A. J.; Schenning, A. P. H. J.; De Greef, T. F. A.; Meijer, E. W. *Nature* **2013**, *481*, 492–496. (c) Kang, J.; Miyajima, D.; Mori, T.; Inoue, Y.; Itoh, Y.; Aida, T. *Science* **2015**, *347*, 646–651.

(18) Cantekin, S.; De Greef, T. F. A.; Palmans, A. R. A. *Chem. Soc. Rev.* **2012**, *41*, 6125.

(19) Mes, T.; Cantekin, S.; Balkenende, D. W. R.; Frissen, M. M. M.; Gillissen, M. A. J.; De Waal, B. F. M.; Voets, I. K.; Meijer, E. W.; Palmans, A. R. A. *Chem. - Eur. J.* **2013**, *19*, 8642–8649.

(20) Roosma, J.; Mes, T.; Leclère, P.; Palmans, A. R. A.; Meijer, E. W. *J. Am. Chem. Soc.* **2008**, *130*, 1120–1121.